



Length scale effects of micro- and meso-scale tensile tests of unirradiated and irradiated Zircaloy-4 cladding

January 2025

Changing the World's Energy Future

Sebastian Lam, David Frazer, Peter Hosemann, Malachi Michael Nelson, Stephanie A Pitts, Brennan K Harris, Fabiola Cappia



DISCLAIMER

This information was prepared as an account of work sponsored by an agency of the U.S. Government. Neither the U.S. Government nor any agency thereof, nor any of their employees, makes any warranty, expressed or implied, or assumes any legal liability or responsibility for the accuracy, completeness, or usefulness, of any information, apparatus, product, or process disclosed, or represents that its use would not infringe privately owned rights. References herein to any specific commercial product, process, or service by trade name, trade mark, manufacturer, or otherwise, does not necessarily constitute or imply its endorsement, recommendation, or favoring by the U.S. Government or any agency thereof. The views and opinions of authors expressed herein do not necessarily state or reflect those of the U.S. Government or any agency thereof.

Length scale effects of micro- and meso-scale tensile tests of unirradiated and irradiated Zircaloy-4 cladding

**Sebastian Lam, David Frazer, Peter Hosemann, Malachi Michael Nelson,
Stephanie A Pitts, Brennan K Harris, Fabiola Cappia**

January 2025

**Idaho National Laboratory
Idaho Falls, Idaho 83415**

<http://www.inl.gov>

**Prepared for the
U.S. Department of Energy
Under DOE Idaho Operations Office
Contract DE-AC07-05ID14517, DE-AC07-05ID14517**

Length scale effects of micro- and meso-scale tensile tests of unirradiated and irradiated Zircaloy-4 cladding

S. Lam^{1*}, D. Frazer², F. Cappia², M. Nelson^{1,2}, S. Samuha³, S. Pitts², B. Harris², P. Hosemann^{4*}

¹Department of Nuclear Engineering, University of California Berkeley, Berkeley, CA, USA

²Idaho National Laboratory, Idaho Falls, ID, USA

³NCRN - Department of Materials Engineering, Be'er-Sheva, Israel

⁴Department of Mechanical Engineering, University of California Berkeley, Berkeley, CA, USA

Corresponding Author: 2521 Hearst Ave, Berkeley, CA 94709, USA

E-mail address: srlam323@berkeley.edu (S. Lam), peterh@berkeley.edu (P. Hosemann)

Keywords: Zircaloy, Fuel Cladding, Tensile Testing, Small Scale Mechanical Testing

DOI: <https://doi.org/10.1016/j.jnucmat.2024.155469>

Abstract

Zircaloy-4 is an essential material for cladding structures within fission-based reactors. To explore the changes in properties measured on differing length scales, FIB-machined micro-scale tensile tests were performed on both irradiated and control groups of Zircaloy-4. This was correlated with tensile testing on femtosecond laser-machined meso-scale specimens. Pronounced size effects were found when varying specimen geometry. Increases in tensile geometry size were associated with a reduction in measured yield stress for both irradiated and unirradiated samples. Meso-scale testing found strength and strain values similar to that of bulk-scale testing.

1. Introduction

Zircaloy-4 is one of the most common cladding materials for fuel rods in nuclear fission reactors due to its low neutron absorption cross-section, high strength, ductility, and corrosion resistance at elevated temperatures in light water reactor (LWR) environments. Typical pressurized water reactor (PWR) Zircaloy-4 tube geometries, which generally have outer diameters of 5-10mm and wall thicknesses of 0.5mm, offer a unique challenge for standard mechanical testing techniques. The tubes have a unique mechanical anisotropy introduced via preferential crystallographic texture of the hexagonal close-packed (HCP) structure and only material produced in a similar fashion delivers accurate tests. Variables such as wall thickness

reduction ratio, forming, and heat treatment significantly alter the microstructure, so it is desirable to use realistic cladding tubes to measure mechanical properties. However, tube geometries present testing challenges compared to flat plates [1]. Common solutions such as the Axial Tube Tension (ATT) and Ring Hoop Tension (RHT) tests, have been used to reflect uniaxial components of in-service conditions [2,3]. While these tests were able to produce a bulk-like response in thin-walled tube materials, they fall short in accurately representing the state of in-service bi-axial stress conditions [2–4]. These drawbacks can be remedied by utilizing finite element models which can correlate the results to pressurized tube testing that more accurately simulates in-service conditions, as demonstrated by Kamerman *et al.* [5].

The Zircaloy-4 thin-walled tube geometry combined with radioactivity created from material neutron activation has created a need for bulk-like mechanical property evaluation using minute radioactive volumes. Macro-scale tensile testing following ASTM E8 guidelines for metallic materials is the industry standard for mechanical testing [6]. However, these geometries are often too large for radioactive materials which are both limited in volume due to reactor irradiation constraints and can exceed worker radiation dose limits. Furthermore a thin-walled tube does not allow such geometries as presented in ASTM E8 guidelines. One approach used to address this challenge is the extrapolation of small-scale mechanical testing (SSMT) results to the bulk scale.

SSMT on the micro-scale has been employed to study fundamental mechanical behaviors for decades. With regard to nuclear materials, this length scale is essential due to the low volume and dosage restrictions. Typical ways to machine micro-scale geometries have included focused ion beam (FIB) milling, electron beam lithography (EBL), and other lithography techniques [7,8]. While fundamental insights into isolated material defects like grain boundaries and precipitates can be gained, extrapolating these results to the bulk-scale has proven to be challenging [9]. Changes in the deformation mechanism and microstructural effects depending on the length scale have to be considered for accurate correlations with bulk scale testing [9,10]. Plastic instabilities are especially sensitive to size effects like grain size, testing geometries, and strain rates [11].

While SSMT samples can be fabricated using FIB or lithography methods, producing samples at this length scale which capture multiple grains on a cladding tube geometry is simply cost and time-prohibitive due to the large dimensions needed compared to the low removal rate of a FIB. Femtosecond laser machining offers a high-throughput method for machining tensile dogbone specimens for mechanical testing. High ablation rates combined with a $<5\mu\text{m}$ heat affected zone (HAZ) create suitable conditions for machining defect free structures on the meso-scale, reducing radioactive exposure doses compared to bulk scale samples [12–14]. While an ASTM standard geometry has not been developed for this length scale, previous studies performed by Dong *et al.*, Harvey *et al.*, and Gigax *et al.* demonstrated that regionally selective bulk-like properties can be obtained on stainless steel alloys using fs-laser machined meso-scale tensile bars [10,15,16]. However a common issue with this meso-scale mechanical testing is that microstructural features such as grain size and micro-texture significantly influence data fidelity

and consistency highlighting a key drawback of this method.

In this work we correlate fs-laser machined meso-scale tensile testing with SSMT data on industrial Zircaloy-4 cladding. Despite the complicated, highly textured Zircaloy-4 cladding microstructure with variable grain sizes, we are able to generate useful bulk-like materials property values using micro- and meso-scale uniaxial tensile testing. This workflow outlines a path towards conducting similar machining and testing procedures on active irradiated samples without the need of large hot cell facilities.

2. Experimental Method

Commercial Zircaloy-4 tubes with a diameter of 9.5mm and wall thickness of 0.57mm were procured with a nominal composition in Table 1. Three tensile geometries were chosen for this study and their dimensions are shown in Figure 1. These include two sizes of micro-scale tensile bars along with a meso-scale geometry. Henceforth, the smaller micro-scale geometry, the larger micro-scale geometry, and the meso-scale geometry will be labeled by their gauge widths: “2 μ m”, “7 μ m” and “80 μ m” respectively for simplicity. The 2 μ m, 7 μ m, and 80 μ m geometries had approximately square gauge cross sections with thicknesses of 2 μ m, 7 μ m and 100 μ m respectively. The 2 μ m and 7 μ m geometries were prepared in the axial direction using a gallium ion FIB and plasma xenon FIB with two varying tensile geometries shown in Figure 1. A total of eight 2 μ m and eleven 7 μ m geometries were FIB produced. In addition to this, four 2 μ m and seven 7 μ m of the tensile bars were made from an irradiated tube of Zircaloy-4. This irradiated tube with an ID of “R-05” was part of the Accident Tolerant Fuels 2 (ATF-2) experiment and was irradiated at the Advanced Test Reactor (ATR) Loop 2A at Idaho National Laboratory (INL). The rod was loaded with UO₂ fuel and irradiated during the period of June 2018 to September 2019 with multiple pauses during testing. This rod was able to achieve a burnup of 9.27 GWd/tHM at temperatures ranging from 250°C to 280°C [2,17,18]. Kamerman et al. calculates this rod’s fast fluence as 1.98×10^{25} n/m² using a coupled Monte Carlo N-Particle (MCNP) and ORIGEN methodology [19]. Rough milling of the SSMT tensile samples was conducted at 30kV and 60-2000nA while final cleaning used 30kV and 0.5-10nA. Both geometries were given a small curvature at the bottom and top of the gauge section to mitigate stress concentration at sharp edges. The final geometry was measured in an SEM to verify dimension and correct the stress measurement. These tensile dogbones were then tested *in-situ* with a Hysitron PI-88 SEM picoindenter equipped with custom FIB-milled tensile shoulder grippers to fit each tensile geometry. The testing was load-controlled at a rate of 10nm/s and videos of each tensile test were recorded. For the micro-scale geometries, the load-displacement data was converted to stress-strain using the final measured gauge dimensions, with no additional processing being performed.

	Zr	Sn	Fe	Cr	O	C	H
%	Bal.	1.22	0.19	0.11	0.13	0.020	0.0017

Table 1. Nominal composition of Zircaloy-4

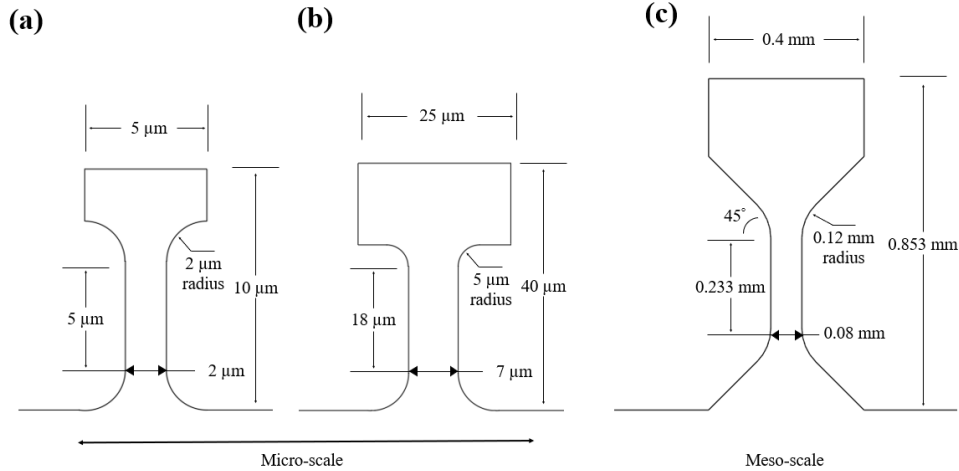


Figure 1. Schematic illustration of all tensile geometries. (a) 2 μm geometry. (b) 7 μm geometry. (c) 80 μm geometry.

The meso-scale 80 μm tensile specimens were prepared from a 100 μm thick foil sample of Zircaloy-4 tubing which was sectioned using a high-speed diamond saw. The sample surface on both sides was polished from 600 grit sandpaper to a final solution of 1 μm diamond suspension. The foil was machined using an 8W Spirit One fs-laser combined with a Newport microfabrication workstation to control movement. The laser system was run at a power of 3W, a laser wavelength of 1040nm, a pulse duration of 332fs, and a repetition rate of 50kHz using a Mitutoyo NIR 10x objective lens which has a focused spot size of $\sim 10\mu\text{m}$. A compressed air gas flow was used to assist in removing ablation particles during cutting. The 80 μm tensile geometry is shown in Figure 1 and the gauge section was machined parallel to the axial direction of the tube to mimic an ATT test. The tensile bars were given a 0.12mm radius curvature at the top and bottom of the gauge section in order to mitigate potential fracture sites at sharp corners. Following laser machining, the tensile bars were quickly immersed in a bath of ethanol in an ultrasonic cleaner to remove excess ablation particles on the surface. Six 80 μm geometries were produced using the fs-laser and each took approximately 3 minutes to fabricate highlighting the rapid ablation rates that can be achieved with this process. A small taper of approximately 3° was observed on all the meso-scale tensile bars due to the lasering process creating a slightly trapezoidal cross-sectional shape which was corrected for in the reported stress. The effect of this taper on deviations in the uniaxial stress state of the tensile bar was mitigated by using laser-machined shoulder grippers which had the same tapering angle, meshing them together. The lasering process also created a small ripple-like texture on the surfaces parallel to the beam which is not expected to affect results and can be seen in Figure 3 [15]. These tensile dogbones

were tested in a Kammrath-Weiss compression and tension module equipped with custom laser-machined shoulder grippers. The tensile tests were run in displacement control at a strain rate of 0.1%/s. For the meso-scale testing, direct image correlation (DIC) was used to correlate the strain and correct for machine compliance. Machine compliance was further corrected by using a material with a known elastic modulus and adjusting the measured strain values accordingly. A 3D visualization of all tensile geometries is shown in Figure 2 and SEM images are shown in Figure 3.

Microstructural examination was performed using a Thermo Fisher Scios 2 DualBeam SEM equipped with an Oxford Symmetry S3 electron backscatter diffraction (EBSD) detector. Prior to examination the surface was mechanically polished from 600 grit sandpaper to a 0.02 μm colloidal silica solution and then cryo-electro polished at 0°C for one minute. Microstructure analysis and visualization were performed using the ATEX software package [20]. We define the normal direction (ND) as the radial axis, the transverse direction (TD) as the hoop axis, and the rolling direction (RD) as the axial axis. The EBSD inverse pole figure (IPF) map was acquired from the ND showing the RD-TD plane.

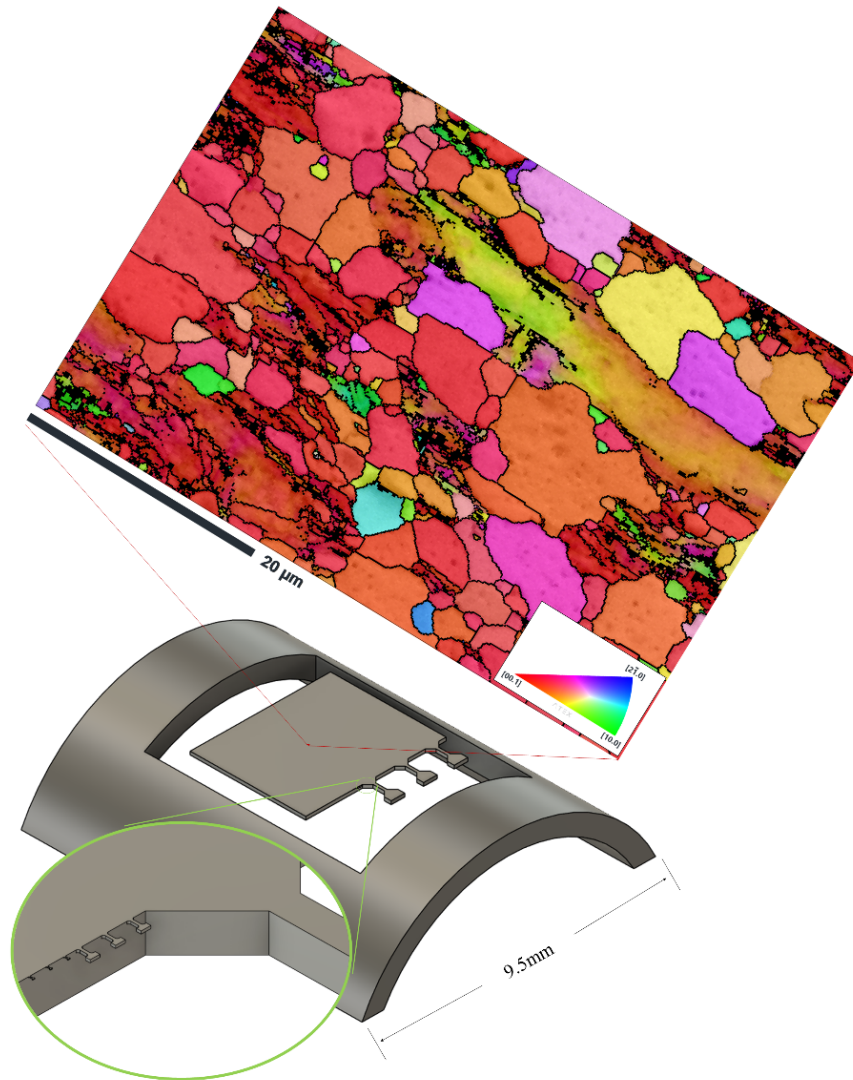


Figure 2. Section of Zircaloy-4 tubing with a scaled schematic illustration of all tensile geometries with EBSD IPF map. A legend color scheme key is presented in the form of a stereographic triangle in the bottom right corner of the EBSD orientation map. For the color representation of this figure, please refer to the web version of this paper. [4].

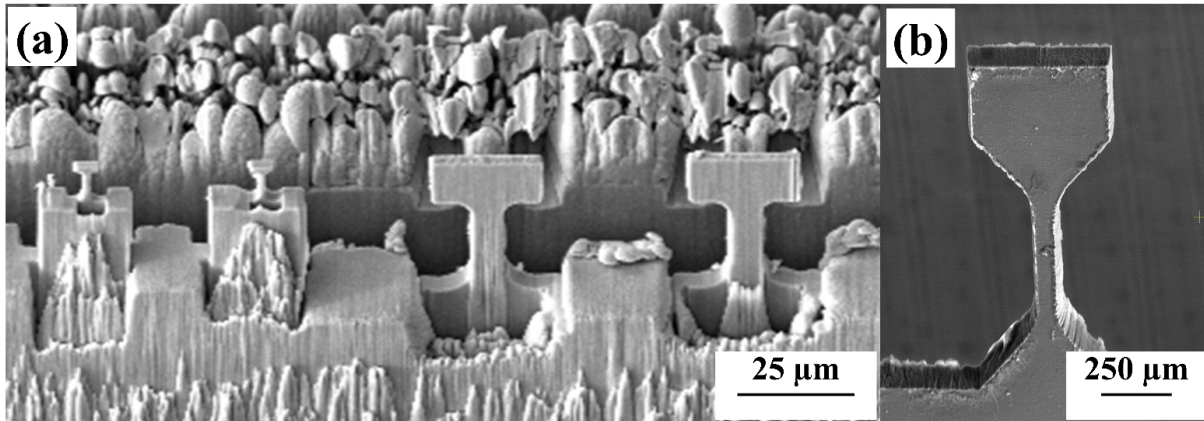


Figure 3. (a) FIB fabricated 2 μ m tensile bars (left) and 7 μ m tensile bars (right). (b) fs-Laser fabricated 80 μ m tensile bars

3. Results

The results of the EBSD scan are shown in Figure 2 using a ND-projection IPF visualizing the texture and grain morphology of the cladding. There is a strong texture in the grains of the tube with a general preference for the basal plane normal oriented parallel to the ND (radial) direction of the tubing. This texture is a result of the pilger processing used on the Zircaloy-4 tubes used to reduce the tube wall thickness. In the paper by Nelson *et al.* which analyzed the same Zircaloy-4 alloy batch it was found that the grain sizes of the tubing followed a bimodal distribution with many islands of fine nanometer scale grains forming within a matrix of larger grains [4,21]. The area-weighted average grain size is 4.83 μ m where grains within two standard deviations fall between 0.44-11.38 μ m. Using this approximation for average grain size, the 2 μ m, 7 μ m, and 80 μ m geometries contained approximately 0.2, 2.7, and 436.6 grains within the gauge area.

The raw load-displacement data for all the tensile testing was converted to stress-strain curves and is displayed in Figure 5. The strain-to-failure was found by visually inspecting the recordings of each tensile test and correlating where fracture initiated, which correlated to a large load drop. From this data, values for 0.2% offset yield stress, ultimate tensile strength (UTS), and strain-to-failure were calculated and are shown in Table 2.

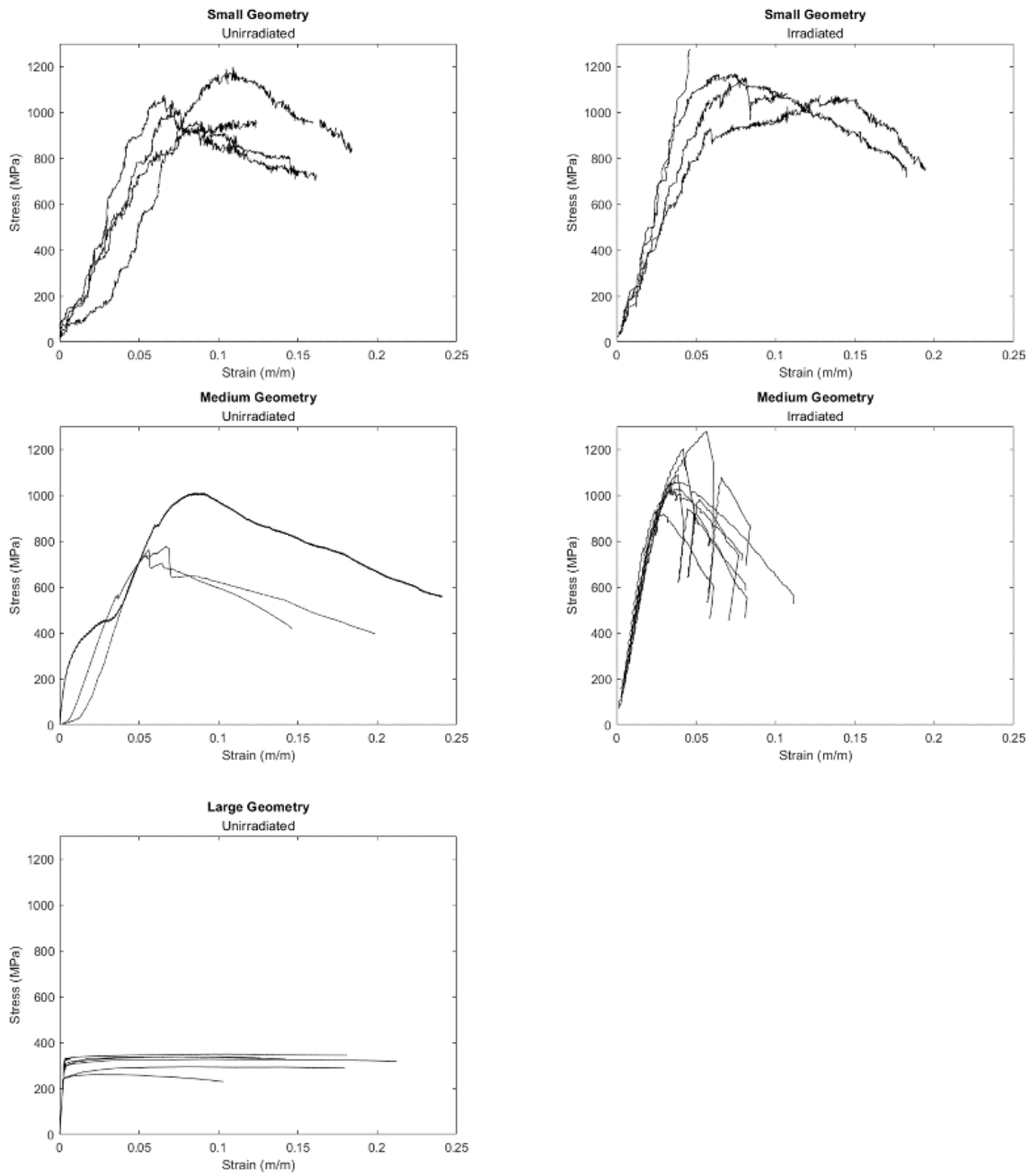


Figure 5. Compiled Zircaloy-4 stress-strain curves to failure for all tensile geometries

Tensile Bar	Length Scale	Gauge Width and Gauge Thickness (μm)	Gauge Length (μm)	Tensile Bars Tested	Yield Stress (MPa) \pm STD	UTS (MPa) \pm STD	Strain to Fracture (m/m) \pm STD
2 μm	Micro-	2	5	4	946.7 \pm 161.2	1069.5 \pm 98.2	0.154 \pm 0.025
2 μm Irradiated	Micro-	2	5	4	1106.6 \pm 130.4	1167.9 \pm 82.2	0.133 \pm 0.069
7 μm	Micro-	7	18	4	737.0 \pm 138.8	851.4 \pm 138.8	0.195 \pm 0.047
7 μm Irradiated	Micro-	7	18	7	877.7 \pm 56.1	1081.9 \pm 110.1	0.082 \pm 0.015
80 μm	Meso-	80	233	6	290.1 \pm 33.0	318.0 \pm 6.74	0.157 \pm 0.040
Reference Bulk Scale (ATT) [2]	Bulk-	570	14500	1	262.5	416.74	0.138
Reference Bulk Scale (ATT) Irradiated [2]	Bulk	570	14500	1	764.5	854.0	0.066

Table 2. Analyzed data for Zircaloy-4 stress-strain curves of all tensile geometries

4. Discussion

Both unirradiated and irradiated 2 μm geometries deformed with similar strain-to-failures and yield stresses, however, some differences in the stress-strain curves can be attributed to irradiation. The yield stress of the irradiation condition is higher, however, both seemed to deform in a largely ductile manner as evidenced by the comparable strains. Macro-scale testing on Zircaloy-4 shows a considerable decrease in strain due to irradiation hardening and embrittlement effects however this trend is not as pronounced [2,22,23].

The deformation behavior of the unirradiated and irradiated 7 μm tensile bars differed significantly. In general, for the irradiated condition, plastic deformation occurred in large, single slip steps seen in Figure 5 and Figure 6 with higher yield stress when compared to the unirradiated condition. This result correlates well with other mechanical testing on irradiated materials and can be attributed to typical irradiation hardening behavior [2,22,23]. Upon closer inspection of the irradiated 7 μm tensile bars, two distinct behaviors were revealed. For four of the seven tensile bars we observe larger strain-to-failure and lower yield strengths while the remaining samples exhibited smaller strain-to-failures, higher yield strengths, and significant strain bursts compared to each other. This can again be explained through the grain size variance in Zircaloy-4. The former of the two behaviors could correlate to the tensile bars which had a finer grain size and were able to serve as effective sinks for radiation defects. The latter of the two behaviors would correlate to coarse-grained tensile bars which experience a loss of plasticity in the grain interior and subsequent large slip steps and strain bursts. In the irradiated material, the presence of a large density of dislocation loops impedes dislocation motion, causing dislocation pileup, and initiating large slip events that presented strain bursts in the irradiated material. In contrast, in the unirradiated condition, plastic deformation occurs through multiple

slip steps resulting in a comparatively gradual decrease in load.

The 80 μm tensile geometry stress-strain curves show a combination of ductile and brittle deformation with small amounts of necking before failure. The fracture surface shown in Figure 6 shows the mixed ductile-brittle fracture mode. The 80 μm geometry's behavior correlates well with bulk scale ATT tests done by Kamerman *et al.* on the same batch of Zircaloy-4 as shown in Figure 7. However, the yield strength of both the 80 μm geometry and bulk testing in Kamerman *et al.* are low when compared to estimates in other studies. With ATT testing of differing geometries, Chu *et al.* measures Zircaloy-4 yield strength to be around 750MPa and Bang *et al.* reported a value of around 550MPa, both with similar strain-to-failure values [24,25]. This difference in measured yield can be attributed to the differing strain rates of testing and processing conditions of the Zircaloy-4 tubes such as the cold work percentage. Another discrepancy in the meso-scale testing from the bulk scale testing done by Kamerman *et al.* is the lower flow stress measured on the meso-scale as evidenced by the lower UTS [2]. This low flow stress can be attributed to the differing strain rates used for testing, a lack of statistics on the bulk scale, and a dramatic decrease in grains sampled on the meso-scale. In particular, the low strain rate used in this testing is commonly correlated with low flow stresses [26].

Lattice and slip system orientations also appear to affect the results. Figure 6(a) shows deformation occurring along a nearly ideal plane at 45° from the tension axis, while Figure 6(b) shows deformation occurring at many angles including normal to the tension axis where very little resolved shear stress is developed. Variations in slip system orientation could develop differences in yield and plastic behavior which is especially significant where one grain orientation provides a majority of the gauge section, such as small gauge sections. This effect is averaged over many grain orientations in larger gauge sections such as the 80 μm gauge sections, and a more consistent yield is observed for the unirradiated 80 μm samples compared to the 7 μm and 2 μm samples in Figure 5.

Comparing all the data, a distinct trend in the yield strength of each stress-strain curve when plotted against tensile bar size shown in Figure 7 is found. There is a clear decrease in the yield strength and UTS of the Zircaloy-4 when tested on a larger length scale which can be attributed to a mix of mechanisms. Dislocation motion governs plasticity in most materials and a reduction in volume of tested material decreases the amount of potential sites for impeded dislocation motion and the accumulation of stress concentrators. Defect-free nanometer scale structures exhibit near theoretical strengths due to the lack of these stress concentrators and the additional energy needed to nucleate dislocations to propagate through the material [9]. Primarily for this study, the amount of grain boundaries sampled changes drastically for the 2 μm , 7 μm , and 80 μm tensile bars. The increase in stress concentrators at a larger length scale contributes heavily to the decrease in observed material strength. These results correlate well with the model proposed by Hosemann *et al.* on the yield strength correlation with length scale [9,27]. The strain-to-fracture found for each length scale was consistent with that of bulk scale testing, but decreased significantly for the 7 μm irradiated condition. This trend of a decreasing strain-to-failure further continues with irradiation on the bulk scale as shown by Kamerman *et al.* [2]. If

the only difference between the length scales tested is the amount of grains sampled, this difference in strains suggests that the mechanisms which cause losses in ductility due to radiation damage are heavily influenced by grain boundaries [28].

While not expected to affect the mechanical data of the meso-scale testing significantly, the effects of some factors inherent to the femtosecond laser process have not been studied in depth. These factors primarily include the redeposition of ablation nanoparticles on the surface of the tensile bars, small ripples formed on the lasered surface, and the development of a small HAZ due to the laser interaction. It is also noted that the ratios of the gauge width to gauge thickness and gauge length to gauge thickness are slightly different between the micro- and meso-scale tensile bars. While this slightly affects the stress state of each tensile bar, it is not expected to greatly affect mechanical results [29].

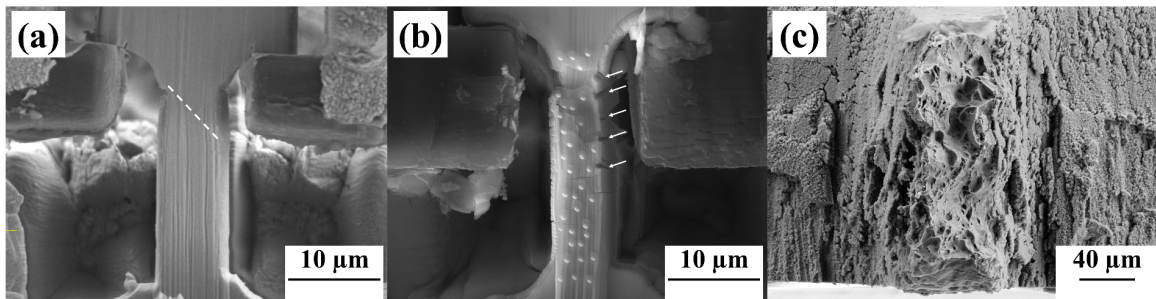


Figure 6. SEM images of tensile fracture. (a) Image of irradiated 7µm tensile bar showing large slip step. (b) Image of unirradiated 7 µm tensile bar showing multiple crack nucleation preferentially at surface. Dots indicate markings intended for Direct Image Correlation (DIC). (c) 80µm tensile bar image of fracture surface showing mixed ductile-brittle fracture.

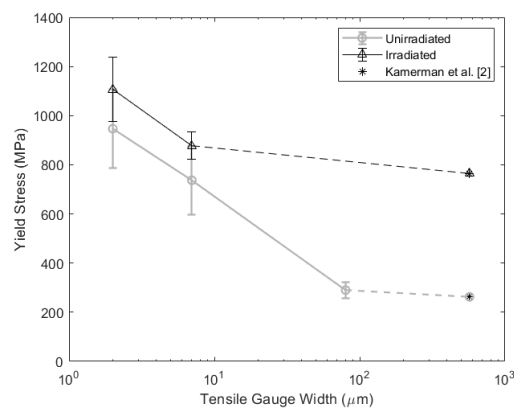


Figure 7. Final yield stress values for both control and irradiated Zircaloy-4 plotted against length scale tested with error bars showing standard deviations

5. Conclusion

Tensile testing was conducted on three different length scales and the mechanical properties were extracted. Irradiated and unirradiated micro-scale tensile specimens were compared to further observe length scale dependency on mechanical properties. Key findings of this study were:

- The yield strength of Zircaloy-4 differed when measured on differing length scales and showed a sharply decreasing trend from micro- to meso-scale. This decrease plateaued with meso-scale testing showing promise in obtaining bulk-like property values with a minimal sample volume. This would require understanding the microstructure of the material and manufacturing tensile bars that contain enough strength determining features to measure bulk properties.
- Irradiated Zircaloy-4 when tensile tested on the micro-scale shows similar trends to that of bulk-scale testing with an increase in yield strength and UTS following irradiation. However for testing the smallest, 2 μ m gauge width, tensile bars, no loss in ductility was found with a similar hardening effect.

The use of fs-laser machining of meso-scale tensile specimens serves as a unique middle ground to sampling bulk-like tensile properties while minimizing the volume of material needed for testing. By reducing the volume of radioactive material needed for testing, this would limit radiation worker dosages and facilitate sample handling. These findings are useful for the planning of post-irradiation experiments (PIE) which could sample bulk-scale properties without the need for large and costly hot-cell facilities.

Declaration of Competing Interest

The authors declare that they have no conflict of interest.

CRedit Authorship Contribution Statement

Sebastian Lam: Investigation, Writing – original draft. **David Frazer:** Conceptualization, Investigation, Writing – Review & Editing. **Fabiola Cappia:** Supervision, Resources. **Malachi Nelson:** Investigation, Writing – Review & Editing. **Shmuel Samuha:** Investigation, Writing – Review & Editing. **Stephanie Pitts:** Supervision, Writing- Review & Editing. **Brennan Harris:** Supervision. **Peter Hosemann:** Conceptualization, Supervision, Writing - Review & Editing.

Acknowledgements

Work supported through the INL Laboratory Directed Research & Development (LDRD) Program under DOE Idaho Operations Office Contract DE-AC07-05ID14517. The United States Government retains and the publisher, by accepting the article for publication, acknowledges that the United States Government retains a nonexclusive, paid-up, irrevocable, world-wide license to publish or reproduce the published form of this manuscript, or allow others to do so, for United States Government purposes.

References

- [1] E. Tenckhoff, Deformation mechanisms, texture, and anisotropy in zirconium and zircaloy, (1988). <https://www.osti.gov/biblio/5932937>.
- [2] D. Kamerman, F. Cappia, K. Wheeler, P. Petersen, E. Rosvall, T. Dabney, H. Yeom, K. Sridharan, M. Ševeček, J. Schulthess, Development of axial and ring hoop tension testing methods for nuclear fuel cladding tubes, *Nuclear Materials and Energy* 31 (2022) 101175. <https://doi.org/10.1016/j.nme.2022.101175>.
- [3] R. Daum, S. Majumda, H. Tsai, T. Bray, D. Koss, A. Motta, M. Billone, Mechanical Property Testing of Irradiated Zircaloy Cladding Under Reactor Transient Conditions, in: *Small Specimen Test Techniques: Fourth Volume*, ASTM International 100 Barr Harbor Drive, PO Box C700, West Conshohocken, PA 19428-2959, 2002: pp. 195–210. <https://doi.org/10.1520/STP10821S>.
- [4] M. Nelson, S. Samuha, D. Kamerman, P. Hosemann, Temperature-Dependent Mechanical Anisotropy in Textured Zircaloy Cladding, *Journal of Nuclear Materials* 595 (2024) 155045. <https://doi.org/10.1016/j.jnucmat.2024.155045>.
- [5] D. Kamerman, M. Nelson, Multiaxial Plastic Deformation of Zircaloy-4 Nuclear Fuel Cladding Tubes, *Nuclear Technology* 209 (2023) 872–886. <https://doi.org/10.1080/00295450.2022.2160174>.
- [6] Standard Test Methods of Tension Testing of Metallic Materials (ASTM E8/E8M), (2016). https://www.astm.org/e0008_e0008m-16a.html.
- [7] B.N. Jaya, M.Z. Alam, Small-scale mechanical testing of materials, *Current Science* 105 (2013) 1073–1099.
- [8] S. Wurster, R. Treml, R. Fritz, M.W. Kapp, E. Langs, M. Alfreider, C. Ruhs, P.J. Imrich, G. Felber, D. Kiener, Novel Methods for the Site Specific Preparation of Micromechanical Structures: Presented at the Metallography Conference 2014 in Leoben, Austria, *Practical Metallography* 52 (2015) 131–146. <https://doi.org/10.3139/147.110331>.
- [9] P. Hosemann, Small-scale mechanical testing on nuclear materials: bridging the experimental length-scale gap, *Scripta Materialia* 143 (2018) 161–168. <https://doi.org/10.1016/j.scriptamat.2017.04.026>.
- [10] A. Dong, J. Duckering, J. Peterson, S. Lam, D. Routledge, P. Hosemann, Femtosecond Laser Machining of Micromechanical Tensile Test Specimens, *JOM* 73 (2021) 4231–4239. <https://doi.org/10.1007/s11837-021-04971-w>.
- [11] T.T. Zhu, A.J. Bushby, D.J. Dunstan, Materials mechanical size effects: a review, *Materials Technology* 23 (2008) 193–209. <https://doi.org/10.1179/175355508X376843>.
- [12] R. Le Harzic, N. Huot, E. Audouard, C. Jonin, P. Laporte, S. Valette, A. Fraczkiewicz, R. Fortunier, Comparison of heat-affected zones due to nanosecond and femtosecond laser pulses using transmission electronic microscopy, *Applied Physics Letters* 80 (2002) 3886–3888. <https://doi.org/10.1063/1.1481195>.
- [13] C. Momma, B.N. Chichkov, S. Nolte, F. Von Alvensleben, A. Tünnermann, H. Welling, B. Wellegehausen, Short-pulse laser ablation of solid targets, *Optics Communications* 129 (1996) 134–142. [https://doi.org/10.1016/0030-4018\(96\)00250-7](https://doi.org/10.1016/0030-4018(96)00250-7).
- [14] A. Mouskeftaras, O. Koritsoglou, G. Duchateau, O. Utéza, From Femtosecond Laser-Induced Plasma Formation Inside Glass to Stress Wave Generation and Propagation: Experiments and Modelling, in: *2023 Conference on Lasers and Electro-Optics Europe & European Quantum Electronics Conference (CLEO/Europe-EQEC)*, 2023: pp. 1–1. <https://doi.org/10.1109/CLEO/Europe-EQEC57999.2023.10231963>.
- [15] C. Harvey, A.J. Torrez, S. Lam, H. Kim, S.A. Maloy, J.G. Gigax, Demonstration of a High-Throughput Tensile Testing Technique Using Femtosecond Laser-Fabricated Tensile Bars in AISI 316 and Additively Manufactured Grade 91 Steel, *JOM* 73 (2021) 4240–4247.

- <https://doi.org/10.1007/s11837-021-04964-9>.
- [16] J.G. Gigax, O. El-Atwani, Q. McCulloch, B. Aytuna, M. Efe, S. Fensin, S.A. Maloy, N. Li, Micro- and mesoscale mechanical properties of an ultra-fine grained CrFeMnNi high entropy alloy produced by large strain machining, *Scripta Materialia* 178 (2020) 508–512. <https://doi.org/10.1016/j.scriptamat.2019.11.042>.
- [17] Kate Richardson, Heather Medema, ADVANCED FUELS CAMPAIGN 2020 Accomplishments, Idaho National Laboratory, 2020.
- [18] F. Cappia, Non-destructive Examinations of ATF-2 Baseline Rodlets, 2020. <https://doi.org/10.2172/1637596>.
- [19] D. Kamerman, B. Durtschi, N. Woolstenhulme, B. Curnutt, T. Labossiere-Hickman, R. Skifton, F. Cappia, An Integral Light Water Reactor Irradiation Experiment for Accident Tolerant Fuel Development, (2023). <https://doi.org/10.2139/ssrn.4341149>.
- [20] Jean-Jacques Fundenberger, Benoit Beausir, Analysis Tools for Electron and X-ray diffraction ATEX-software, (2017).
- [21] M. Nelson, S. Samuha, B. Kombaiyah, D. Kamerman, P. Hosemann, Enhanced stress relaxation behavior via basal $\langle a \rangle$ dislocation activity in Zircaloy-4 cladding, *Journal of Nuclear Materials* 601 (2024) 155337. <https://doi.org/10.1016/j.jnucmat.2024.155337>.
- [22] C.L. Whitmarsh, REVIEW OF ZIRCALLOY-2 AND ZIRCALLOY-4 PROPERTIES RELEVANT TO N.S. SAVANNAH REACTOR DESIGN, 1962. <https://doi.org/10.2172/4827123>.
- [23] A. Hermann, M. Martin, P. Porschke, S. Yagnik, DUCTILITY DEGRADATION OF IRRADIATED FUEL CLADDING, (n.d.).
- [24] H.C. Chu, S.K. Wu, K.F. Chien, R.C. Kuo, Effect of radial hydrides on the axial and hoop mechanical properties of Zircaloy-4 cladding, *Journal of Nuclear Materials* 362 (2007) 93–103. <https://doi.org/10.1016/j.jnucmat.2006.11.008>.
- [25] S. Bang, H. Kim, J. Noh, D. Kim, K. Keum, Y. Lee, Temperature-dependent axial mechanical properties of Zircaloy-4 with various hydrogen amounts and hydride orientations, *Nuclear Engineering and Technology* 54 (2022) 1579–1587. <https://doi.org/10.1016/j.net.2021.11.007>.
- [26] W.F. Hosford, ed., Strain-Rate and Temperature Dependence of Flow Stress, in: *Solid Mechanics*, Cambridge University Press, Cambridge, 2010: pp. 84–101. <https://doi.org/10.1017/CBO9780511841422.007>.
- [27] P. Hosemann, C. Shin, D. Kiener, Small scale mechanical testing of irradiated materials, *J. Mater. Res.* 30 (2015) 1231–1245. <https://doi.org/10.1557/jmr.2015.26>.
- [28] R. Roy, F. Long, M.R. Daymond, A mechanistic study of grain boundary behaviour during irradiation-induced growth in zirconium, *Acta Materialia* 276 (2024) 120075. <https://doi.org/10.1016/j.actamat.2024.120075>.
- [29] A. Dong, H. Vo, E. Olivas, J. Bickel, C. Hardie, P. Hosemann, S. Maloy, The effect of sample thickness on micro-mesoscale tensile properties of 304SS, HT-9, and CuCrZr, *Journal of Nuclear Materials* 575 (2023) 154207. <https://doi.org/10.1016/j.jnucmat.2022.154207>.